Through-grid wicking enables high-speed cryoEM specimen preparation

Yong Zi Tan[1] and John L. Rubinstein[1,2,3,*]

[1.] Molecular Medicine Program, The Hospital for Sick Children, Toronto, Ontario, Canada
[2.] Department of Biochemistry, The University of Toronto, Ontario, Canada
[3.] Department of Medical Biophysics, The University of Toronto, Ontario, Canada
* Correspondence: john.rubinstein@utoronto.ca

Abstract

Blotting times for conventional cryoEM specimen preparation complicate time-resolved studies and lead to some specimens adopting preferred orientations or denaturing at the air-water interface. We show that solution sprayed onto one side of a holey cryoEM grid can be wicked through the grid by a glass fiber filter held against the opposite side, often called the 'back' of the grid, producing a film suitable for vitrification. This process can be completed in tens of milliseconds. We combined ultrasonic specimen application and through-grid wicking in a high-speed specimen preparation device that we name "Back-it-up", or BIU. The high liquid-absorption capacity of the glass fiber compared to self-wicking grids appears to make the method relatively insensitive to the amount of sample applied. Consequently, through-grid wicking produces large areas of ice suitable for cryoEM, while the device's speed reduces adoption of a preferred orientation in a test specimen.

Introduction

Advances in single particle electron cryomicroscopy (cryoEM) now allow routine high-resolution structure determination for many macromolecules and molecular assemblies. Nonetheless, the ability to prepare specimens suitable for imaging remains one of the main bottlenecks for these structural studies. Standard specimen preparation methods (*1*, *2*) involve using a micropipette or syringe to transfer microliter volumes of solution onto the surface of an EM grid coated with a holey carbon or gold film (Fig. 1*A*). Excess sample is removed by blotting with paper for seconds to produce a thin aqueous film, which is subsequently vitrified by plunging the grid into a cryogen such as liquid ethane or a mixture of liquid ethane and liquid propane. The liquid-absorption capacity of the paper is far larger than the amount of sample applied, suggesting that blotting for too long should lead to complete drying of the grid. However, once formed, these thin films of solution appear to be moderately stable, with continued blotting only slowly thinning the film (*3*). This continued thinning could occur either through further wicking or through evaporation.

Blotting with paper can be done from one or both sides of the grid. If blotting is performed from only one side, it is usually done on the side where the sample was applied. 'Backside blotting', where sample is applied on one side and blotting is performed on the other, has been used to concentrate filaments or particles that cannot pass through the grid holes (*4*). Blotting a 3 µL sample into a 1000 Å thick film that covers a 3 mm diameter EM grid requires removal of 99.998% of the liquid. Consequently, blotting to remove sample without concentrating the molecule of interest on the grid is extraordinarily wasteful. The time required to prepare a thin film by blotting, which is likely due to the large volume of liquid that must be removed, prevents or complicates using grid freezing to study time dependent processes that occur on timescales shorter than a few seconds. During grid preparation, the sample exists as a thin liquid film with a large surface area to volume ratio, exposing fragile macromolecules to nearby hydrophobic air-water interfaces for an extended period. The interaction of protein particles with an air-water interface has been found to induce preferred orientations for many specimens (*5*) and cause denaturation of others (*6*, *7*).

55

56 The introduction of self-wicking grids (*8*, *9*) provided a new way of preparing cryoEM
57 specimens (Fig. 1*B*). With these specimen supports, copper hydroxide nanowires are grown from
58 the copper surface of copper-rhodium grid bars by incubating the grids in a solution of
59 ammonium persulfate at basic pH. The grids are subsequently covered with a sacrificial film of
60 holey plastic (*8–10*) that can be coated with carbon or gold before the plastic is dissolved. During
61 specimen freezing, small volumes of liquid are applied onto the nanowire side of the grid. When
62 the liquid contacts the nanowires, most of the sample is wicked to the grid bars, leaving a thin
63 film suitable for vitrification and subsequent imaging. The volume of liquid applied is small and
64 the wicking process occurs quickly, producing a suitable film in tens of milliseconds. However,
65 the nanowires on the grid have a limited capacity to absorb liquid and can be easily saturated if
66 too much sample is applied. Further, the speed of wicking from copper hydroxide-nanowire grids
67 can vary from grid to grid, a problem thought to be due to variability in the copper used to make
68 the grids (*9*). The small droplets of liquid needed for this approach have been generated
69 previously by two different methods, although presumably other liquid dispensing techniques
70 could also be used. In the first application of self-wicking grids, a piezoelectric transducer
71 coupled to a glass capillary, similar to the printing head in an inkjet printer, was used to apply
72 sample (*11*, *12*). This device, named "Spotiton", led to the commercial "Chameleon" instrument
73 from SPT Labtech Ltd (*13*). With Spotiton and Chameleon, the sample is applied onto a strip of
74 grid squares as the grid as it is moved past the dispensing head, allowing the wicking behavior of
75 the grid to be characterized with high-speed cameras. Suitable conditions are selected and the
76 sample is applied to a different strip of grid squares on the same grid before plunge-freezing in
77 cryogen. This approach requires high-precision liquid dispensing and high-quality optical
78 components. Alternatively, liquid can be dispensed in a less controlled manner by a simple
79 piezoelectric transducer like the ones found in ultrasonic humidifiers, an approach implemented
80 with the open-source "Shake-it-off" (SIO) device (*14*). This device relies on the piezoelectric
81 transducer producing a distribution of droplets that varies in intensity across the grid so that
82 some regions are saturated with liquid, some are dry, and some receive an optimal volume to
83 produce ice of an appropriate thickness for imaging.
84

85 A drawback of the Shake-it-off device is that it tends to produce only small areas of usable ice,
86 with significant variation from grid to grid. Therefore, we sought to develop a robust approach
87 for cryoEM grid preparation with the speed of self-wicking grids, but with the simplicity of
88 conventional grid preparation. We reasoned that the large excess of absorption capacity during
89 conventional grid preparation allows the process to reach the metastable state of a thin film
90 regardless of the exact volume of sample applied to the grid. We hypothesized that if liquid
91 could wick through a grid, a large absorption capacity available on one side of a holey grid
92 would allow specimens to be prepared by high-speed application of small volumes of liquid to
93 the other side (Fig. 1*C*). The large absorption capacity would make the technique insensitive to
94 the precise volume of liquid applied, enabling large areas of specimen to be prepared for cryoEM
95 with a simple, robust, and inexpensive droplet generator. We found that this effect could be
96 achieved by treating both surfaces of the grid with extensive glow discharge in air to make them
97 hydrophilic and using glass fiber to wick excess solution through the grid. Following the naming
98 pattern of the Spotiton and Shake-it-off devices, and recognizing the similarity to the backside
99 blotting approach, we name the device presented here *"*Back-it-up*"* or BIU.
100
101 **Results and Discussion**
102 *Through-grid wicking with glass fiber allows preparation of thin vitreous ice*
103 We investigated the capability of different blotting materials to rapidly wick liquid through a
104 holey grid when applied to the opposite side of the grid. We found that this effect could be
105 achieved consistently with glass fiber filters but not with conventional filter paper. Glass fiber
106 filters have been used previously to prepare cryoEM specimens from carbon nanotubes in
107 chlorosulfonic acid (*15*). Scanning electron microscopy (SEM) with secondary electron detection
108 illustrates the relatively large cellulose fibers in conventional filter paper (Fig. 2*A*i) compared to
109 the smaller glass fibers (Fig. 2*A*ii). Conventional cryoEM grids with a holey gold film on the
110 rhodium surface of copper-rhodium grids were made hydrophilic by extensive glow discharge in
111 air on both sides and laid with their flat gold surface in contact with either conventional filter
112 paper or a glass fiber filter. A high-speed video of water being applied to the copper surface of
113 the grids shows that the liquid is rapidly wicked through the grid by glass fiber, while this
114 phenomenon did not occur consistently with conventional filter paper (Fig 2*B*; Movie S1).
115

116 To test if through-grid wicking with glass fiber allows production of thin films of vitreous ice
117 suitable for cryoEM, a specimen of commercially available recombinant hemagglutinin trimer
118 from influenza A virus (Strain A/Hong Kong/1/1968[H3N2]) was prepared with a Gatan
119 Cryoplunge 3 (CP3) grid freezing device. After application of sample to the copper surface of the
120 grid, one sided blotting was performed on the gold surface, with the usual 20 mm circle of filter
121 paper replaced with a 20 mm circle of glass fiber filter. The majority of the 3 µL sample
122 appeared to wick through the grid in ~1 sec and blotting was continued for a total of 5 sec. A
123 cryoEM atlas of the grid showed a gradient of ice thicknesses (Fig. 2*C*i), with many grid squares
124 having ice suitable for data collection (Fig. 2*C*ii). High magnification images (Fig. 2*C*iii) of
125 holes with appropriate ice for data collection revealed high-contrast particles similar to
126 micrographs obtained previously with the same hemagglutinin specimen (*16*).
127
128 *Construction of BIU, a high-speed through-grid wicking specimen preparation device*
129 To develop a device that dispenses small volumes of sample for high-speed cryoEM specimen
130 preparation using the through-grid wicking approach, we adapted the open source Shake-it-off
131 platform (*14*) (Fig. 1*C*, 3*A*). In the new instrument design (Fig. 3), Dumont L5 tweezers holding
132 an EM grid are attached with a magnetic connector to a large solenoid capable of plunging the
133 grid into a cryogen bath. The cryogen bath, which is insulated by a Styrofoam box, is milled
134 from aluminum and uses liquid nitrogen to maintain a ~60:40 mixture of propane:ethane in a
135 liquid state (*17*). The ~30 mm travel distance of the plunging solenoid when energized is reduced
136 to ~16 mm by a 3D-printed plastic ring and a magnetic catch keeps the solenoid in its extended
137 position after it is de-energized. A new plastic process mount was designed and 3D-printed to
138 orient the components necessary for through-grid wicking (Fig. 3*B*). On one side of the grid, a
139 wicking assembly (Fig. 3*C*) uses a tack and a magnet to hold a 20 mm diameter circle of glass
140 fiber filter that is supported by a thin flexible circle of cellulose acetate. This wicking assembly
141 is attached to a small solenoid on the plastic mount so that in its energized position the glass fiber
142 filter is held flush against the grid (Fig. 3*D*i). On the other side of the grid the plastic mount
143 holds a 16 mm diameter piezoelectric transducer from an ultrasonic humidifier (Fig. 3*E*). The
144 piezoelectric transducer produces a spray of small droplets when a high-frequency signal is
145 applied by the humidifier circuit. A magnet embedded in the Styrofoam insulating box of the
146 cryogen container is held against a reed switch when the box is properly positioned, serving as a

147 safety interlock to prevent premature plunging of the tweezers. The system electronics are
148 controlled, via a custom printed circuit board identical to the one use with the Shake-it-off
149 device, by a Raspberry Pi single board computer running a graphical user interface (GUI) written
150 in *Python3*.
151
152 During specimen preparation, a small volume of sample, such as a few hundred nL to 1 μL, is
153 applied to the surface of the piezoelectric transducer opposite the grid. Energizing the high-
154 frequency generating circuit causes a spray of droplets through the piezoelectric transducer onto
155 the copper surface of the grid. After spreading on the grid, liquid is wicked through the grid by
156 the glass fiber filter. Once spraying is complete, the glass fiber filter is held against the grid for
157 an additional wicking time (e.g. 10 msec), after which the glass fiber filter and acetate are pulled
158 back from the grid by de-energizing the small solenoid (Fig. 3*D*ii). The large solenoid is then
159 energized and the grid is plunged into the liquid cryogen. At present, this process is carried out at
160 ambient temperature and humidity. However, we see no reason why the BIU device could not be
161 built in a humidity- and temperature- controlled environment, or any number of other controlled
162 environments for specific experiments. Because there is no splash shield for the cryogen, eye
163 protection must always be worn when operating the device. The piezoelectric transducer
164 produces an aerosol from the sample and consequently the device should not be used to prepare
165 samples where aerosols present a health hazard, such as infectious virus particles, some toxins,
166 and infectious prions. However, the device can be installed in a biosafety cabinet to overcome
167 this limitation.
168
169 *High-resolution 3D reconstruction from a specimen prepared with the* BIU *device*
170 In order to determine if the BIU device is able to prepare specimens amenable to high-resolution
171 cryoEM, we used it to prepare multiple grids with human light chain apoferritin. Spraying was
172 done with the piezoelectric transducer energized for 100 msec, with an additional 100 msec
173 delay after spraying and before plunging. This spraying time is twenty times longer than was
174 used with the Shake-it-off device with self-wicking grids and is sufficient to completely saturate
175 copper-hydroxide nanowire grids, leading to thick ice (*14*). CryoEM atlases of the resulting
176 specimen grids show a gradient of ice thicknesses (Fig. 4*A*, *upper*). This gradient could be due to
177 spatial variation in the amount or droplet size of the spray from the piezoelectric transducer on

178 different parts of the grid. Alternatively, it could be due to the gradient of pressure with which
179 the glass fiber filter is pressed against the grid, with less pressure near the edge of the glass fiber
180 filter circle and more pressure where the glass fiber filter is secured to the wicking assembly by
181 the tack. Nonetheless, grids consistently had approximately one third of the their surface covered
182 with ice suitable for imaging. Apoferritin particles can be seen clearly in high-magnification
183 images from multiple grids (Fig. 4*A*, *lower*), demonstrating that the device reproducibly
184 produces specimens with large areas of thin vitreous ice suitable for data collection. A dataset of
185 3,168 movies was collected from two of the grids (Table S1), allowing calculation of a 3D map
186 at 2.0 Å from 594,259 single particle images (Fig. 4*B* to *E*). An atomic model was built into the
187 density map, including water molecules that could be resolved clearly (Fig. 4*E*), confirming that
188 the BIU device is capable of preparing samples that can be used for high-resolution structure
189 determination.
190
191 *High-speed through-grid wicking can reduce time-dependent preferred orientations*
192 With the Spotiton device and self-wicking grids, the influenza A hemagglutinin trimer was
193 shown to undergo time-dependent adoption of a preferred top-view orientation at the air-water
194 interface during grid freezing (*5*). This preferred orientation prevents calculation of a 3D map. In
195 that study, conventional use of a Gatan CP3 (~1 sec blot time) resulted in most particles adopting
196 the three-fold symmetric top views and only 4% of particle images assigned to classes that show
197 a side view of the trimer. In contrast, the number of particle images contributing to side view
198 classes increased to 9% with the Spotiton device and a 500 msec spot-to-plunge time, and to
199 19% with a 100 msec spot-to-plunge time (*5*).
200
201 To determine if specimen preparation with through-grid wicking can be performed at sufficient
202 speed to reduce adoption of preferred orientations, grids were prepared with the BIU device
203 using the identical recombinant hemagglutinin trimer. Sample was sprayed onto the grid with the
204 piezoelectric transducer energized for 30 msec, with an additional 30 msec delay after spraying
205 and before plunging to allow wicking of excess solution by the glass fiber filter. Recording this
206 process at 480 fps (frames per second) showed that the piezoelectric circuit was active for ~45
207 msec, followed by an additional ~30 msec where the grid remained in contact with the glass fiber
208 filter, and ~60 msec passing during which the glass fiber filter was fully retracted and the grid

plunged into cryogen (Fig. 5*A*, Movie S2). This sequence constitutes an overall process time of 135 msec, with immersion in cryogen occurring 90 msec after the end of spraying and 60 msec after breaking contact between the grid and glass fiber filter. 1,556 movies were acquired from this specimen. As with the apoferritin specimens, approximately one third of the grid had ice that was suitable for imaging. 1,284 movies were also acquired from a sample of the hemagglutinin trimer, described earlier, that was prepared using the Gatan CP3 with glass fiber filter paper and backside blotting. With the Gatan CP3 and a 5 sec blot time, 2% of particle images (1,506 out of 91,879) were assigned to a single class corresponding to a side view, while 98% (90,373 out of 91,879) were assigned to classes that showed top views or oblique views (Fig. 5*B*). In contrast, with the BIU grid 66% of particle images (170,419 out of 256,303) were assigned to top or oblique view classes while 34% (85,884 out of 256,303) were assigned to side-view classes (Fig. 5*B*). The top and oblique views for the BIU specimen also appeared to include more tilted oblique views than for the Gatan CP3 specimen (Fig. 5*B*, *left*). The large number of single particle images presenting side views in the BIU specimen allowed 3D reconstruction of the hemagglutinin trimer at 2.9 Å resolution (Fig. 5*C*, 5*D*, Table S1) without the need for tilting the specimen (*16*). The high quality of the map allowed construction of an atomic model, including three N-linked glycans (Fig. 5*E, bottom-right*). The map has a sampling compensation factor (*18*) of 0.92 and a 3D Fourier shell correlation sphericity (*16*) of nearly 1.00 when calculated either between half-maps or between the map and the model (Fig. 5*C*) (Table S1). These statistics support the directional isotropy of the resolution. Local resolution in the map is slightly worse near the membrane proximal part of the trimer (Fig. 5*E, bottom of reconstruction*) as was suggested previously for this complex (*19*), likely due flexibility in the structure.

Discussion

Implementation of through-grid wicking for high-speed cryoEM specimen preparation allows grids to be frozen in tens of milliseconds, rather than the multiple seconds needed for conventional grid preparation. The method does not require the self-wicking nanowire grids used previously in the Spotiton, Chameleon, and Shake-it-off devices. Avoiding nanowire grids and using conventional holey cryoEM grids simplifies the consumables needed for grid preparation and reduces a source of variability that has affected specimen preparation with nanowire grids (*9*). By providing a high capacity for absorbing liquid, through-grid wicking appears to increase

240 the tolerance for excess-liquid applied to the grid. This decrease in sensitivity avoids creation of
241 large areas of ice that are too thick for data collection, even when approximately six to twenty
242 times the spraying time of the Shake-it-off device (*14*) is used with the BIU device, or 3 µL of
243 sample is applied directly to the grid in the Gatan CP3. As a result, large areas of high-quality ice
244 can be prepared readily and reproducibly with the BIU device, with approximately one third of
245 the grid surface available for data collection. This large usable area allows for straightforward
246 structure determination from a single grid.
247
248 Electron tomography of specimens prepared with the Spotiton device showed that the
249 mechanism for reducing preferred orientations was decreased interaction with the thin film air-
250 water interface before freezing (*5*). Although repeating the mechanistic analysis of this effect
251 with the BIU device is beyond the scope of the present manuscript, which instead focuses on the
252 ability of the approach to prepare usable specimens, the abundance of hemagglutinin trimer side
253 views is presumably due to the same effect that occurs when performing high-speed grid
254 preparation with self-wicking grids.
255
256 In the experiments described above we used the same ultrasonic specimen application approach
257 employed with the Shake-it-off instrument, which is related to an acoustic wave atomization
258 approach described previously (*20*). However, through-grid wicking can almost certainly be used
259 with other methods for applying sample onto an EM grid. The piezoelectric transducer from an
260 ultrasonic humidifier used here has the advantage of having no 'dead volume' of sample that
261 must be loaded into the device but cannot be dispensed. It has the disadvantage of using
262 relatively large volumes for each grid, such as hundreds of nanoliters up to one microliter,
263 although it may be possible to reduce this volume further. Alternative sample application
264 methods include the ink-jet approach implemented in the Spotiton device (*11*, *12*) and the
265 microfluidic sprayers used with several time-resolved specimen preparation devices (*21–24*).
266 Through-grid wicking could also prove useful for preparing optimal ice when applying nanoliter
267 samples to a grid with a microcapillary (*25*, *26*) or from a solid surface.
268
269 Similar to the Shake-it-off platform on which it is based, the BIU instrument is inexpensive to
270 construct. The implementation described here cost ~C$1,000 (~USD$700) to build, or

approximately 500 to 1000× less than a commercially available second-generation grid preparation device. All components needed to build the device are either commercially available or can be made by online 3D printing, printed circuit board fabrication, and CNC milling services, so that specialized manufacturing infrastructure is not required. The 3D design files, the printed circuit board design files, and the control software are available online to allow others to easily replicate the instrument (https://github.com/johnrubinstein). We believe that the reproducibility and large areas of usable ice from through-grid wicking, combined with the simplicity and low construction cost of the BIU device, provides a robust and easily accessible approach to high-speed cryoEM specimen preparation.

Author contributions

JLR devised the grid preparation approach, built the instrument, and wrote the control software. YZT devised the characterization strategy, prepared samples, collected data, performed image analysis, and constructed atomic models. JLR and YZT wrote the manuscript and prepared the figures

Acknowledgements

Recombinant human apoferritin was a gift from Taylor Sicard and Jean-Philippe Julien (The Hospital for Sick Children). We thank Ali Darbandi (The Hospital for Sick Children) for performing the SEM imaging in Figure 2. YZT was supported by a postdoctoral fellowship from the Canadian Institutes of Health Research and JLR was supported by the Canada Research Chairs program. This work was supported by a Discovery Grant from the Natural Sciences and Engineering Research Council. CryoEM data was collected at the Toronto High-Resolution High-Throughput cryoEM facility, supported by the Canada Foundation for Innovation and Ontario Research Fund.

Declaration of interests

YZT and JLR have filed a patent application related to the specimen preparation approach described in this manuscript.

Data availability

All raw movies, micrographs, particle stacks, and relevant metadata files will be deposited into EMPIAR. All cryoEM maps will be deposited into the EMDB and atomic models in the PDB. Original software and 3D design files are available from https://github.com/johnrubinstein

Figure 1. Cartoon of different wicking approaches for cryoEM specimen preparation approaches. (*A*) Conventional specimen preparation: the sample is applied to the grid and blotted with filter paper to produce a thin film suitable for plunge freezing. (*B*) Self-wicking grids: nanowires on the grid absorb excess liquid to produce a thin film. Small volumes of the sample are applied by a piezoelectric inkjet dispenser (Spotiton) or piezoelectric transducer (Shake-it-off). (*C*) Through-grid wicking: the sample is applied to one side of the grid while a filter on the other side removes excess sample to produce the film that will be vitrified.

Figure 2. Through-grid wicking with glass fiber. (*A*) Scanning electron microscopy (SEM) images of conventional filter paper (i) and glass fiber filter (ii) at two magnifications. (*B*) A holey gold grid previously subjected to glow discharged on both sides does not consistently show rapid through-grid wicking when in contact with filter paper (i) but water quickly wicks through the grid when it is placed on a glass fiber filter (ii). Movie S1 shows this process in more detail. (*C*) A hemagglutinin trimer specimen prepared by through-grid wicking with a Gatan CP3 grid freezing device and glass fiber filter. A grid atlas (i), grid square (ii), and high magnification image (iii) are shown.

Figure 3. The Back-it-up (BIU) device. (*A*) Fully assembled BIU specimen-preparation device. In comparison with the SIO device, new components are the process mount (*B*) and wicking assembly (*C*). (*D*) When the position solenoid is energized the wicking assembly holds the glass fiber filter flush against the grid to allow spraying and through-grid wicking (i). When the position solenoid is de-energized, the glass fiber filter is retracted creating the clearance needed to plunge the grid into cryogen (ii). (*E*) The back of the piezoelectric transducer shows where the sample is applied before spraying.

Figure 4. Human apoferritin vitrified using BIU. (*A*) Grid atlases, grid squares, and micrographs from human apoferritin prepared for cryoEM using BIU. (*B*) Representative 2D class averages. (*C*) Fourier shell correlation (FSC) curves for apoferritin show the map resolution from half-map (blue) and map-to-model (purple) correlation at FSC=0.143 and FSC=0.5, respectively. A histogram of directional resolutions sampled evenly over the 3DFSC (yellow) is also shown and the corresponding sphericity is indicated. (*D*) Local resolution for the apoferritin reconstruction. (*E*) A representative α helix from the apoferritin model (residues 14 to 41) and the experimental density map (grey surface). Water molecules are displayed as red spheres.

Figure 5. BIU enables fast vitrification, reducing preferred orientation of a hemagglutinin trimer. (*A*) The complete set of 2D class averages from hemagglutinin trimer specimens prepared with the Gatan CP3 and BIU. The fraction of particle images contributing to top and oblique view classes versus side view classes is indicated. (*B*) Fourier shell correlation (FSC) curves show the map resolution from half-map (blue) and map-to-model (purple) correlation at FSC=0.143 and FSC=0.5, respectively. A histogram of directional resolutions sampled evenly over the 3DFSC (yellow) is also shown and the corresponding sphericity is indicated. (*C*) Local resolution map of the hemagglutinin reconstruction. (*D*) A representative α helix (residues 405-454), β sheet (residues 154-175, 195-228, 238-251), and N-glycan (residues 165) from the hemagglutinin model shown as sticks, overlaid with the experimental density map (grey surface).

Movie S1. Comparison of filter paper and glass fiber filter for through-grid wicking. Water (5 μL) applied to a hydrophilic holey gold grid does not consistently wick through the grid when it is placed on filter paper (top) but quickly wicks through the grid when it is placed on a glass fiber filter (bottom).

Movie S2. High speed video of the BIU process. A video recorded at 480 frames per second shows the high-frequency generating circuit of the piezoelectric transducer energized for ~45 msec. A further 30 msec elapses where the glass fiber filter remains in contact with the grid. The grid is plunged into cryogen ~60 msec after it breaks contact with the glass fiber filter.

363 **Table S1. Cryo-EM data collection and modeling statistics**

	Human L Chain Apoferritin (BIU)	Hemagglutinin (CP3)	Hemagglutinin (BIU)
EM data collection / processing			
Microscope	FEI Titan Krios		
Voltage (kV)	300		
Camera	Falcon 4		
Mode	Counting		
Defocus mean ± std (μm)	0.7 ± 0.4	2.0 ± 0.5	2.0 ± 0.5
Exposure time (s)	9	9	9
Number of fractions	29	29	29
Exposure rate (e^-/pixel/s)	3	5	5
Total exposure ($e^-/Å^2$)	40	40	40
Pixel size (Å)	0.816	1.03	1.03
Number of micrographs	3,168	1,284	1,556
Number of particles (after cleanup)	673,794	232,841	378,143
Number of particles (in final map)	594,259	-	128,305
Symmetry	O	-	C3
Resolution (global) (Å)	2.0	-	2.9
Local Resolution Range	1.8-2.2	-	2.5-3.4
Directional Resolution Range	1.9-2.1	-	2.7-3.2
Sphericity of 3DFSC	0.98	-	0.98
SCF Value*	1.00	-	0.92
Map B factor ($Å^2$)	92.8	-	150.9
Model statistics			
Residue range	5-176	-	9-325, 334-501
Map CC	0.88	-	0.77
RMSD [bonds] (Å)	0.006	-	0.011
RMSD [angles] (Å)	1.003	-	1.194
All-atom clashscore	0.14	-	2.45
Average B factors ($Å^2$)		-	
Protein	14.91	-	72.39
Ligands	23.45	-	69.53
Water	16.18	-	-
Ramachandran plot		-	
Favored (%)	98.82	-	93.56
Allowed (%)	1.18	-	6.03
Outliers (%)	0.00	-	0.42
Rotamer outliers	0.00	-	0.94
C-β deviations	0.00	-	0.00
MolProbity Score	0.53	-	1.45
EM-Ringer Score	7.70	-	4.07

364 *The sampling compensation factor (SCF) value is calculated as described (*18*) and assumes that all orientations
365 have been determined accurately.

Materials and Methods

Device design, construction, and consumables

New 3D parts were designed with *Autodesk Fusion 360* and printed in polylactic acid with a Raise3D Pro2 3D printer. All other parts and components were identical to those used with the SIO device (*14*). 20 mm circles of glass fiber filters (VWR grade 691) and filter paper (Whatman #1) were cut with the circle punch from the Gatan CP3 grid freezing device. Nanofabricated holey gold film coated EM grids with regularly spaced ~2 µm holes were prepared on EMS Maxtaform 400 mesh Cu/Rh grids as described previously (*10*). Grids were glow discharged in air for two minutes on each side with a PELCO easiGlow (Ted Pella) immediately before use.

Apoferritin specimen preparation

Human apoferritin light chain (UniProtKB: P02792), modified with an N-terminal Strep tag and linker, a C-terminal extension, and a K173R mutation, was a gift from Taylor Siccard and Jean-Philippe Julien (The Hospital for Sick Children). Apoferritin was diluted to 5 to 10 mg/mL for specimen preparation with BIU. Sample (1 µL) was applied to the piezoelectric transducer and liquid was transferred to the grid by energizing the high-frequency generating circuit for 100 msec. An additional 100 msec was allowed for the glass fiber filter to wick sample through the grid before retracting the filter and plunging the grid into the liquid propane/ethane bath.

Hemagglutinin specimen preparation

Hemagglutinin (MyBioSource product MBS434205) was used without dilution (1 mg/mL). For specimen preparation with the Gatan Cryoplunge 3, sample (3 µL) was applied onto the copper side of nanofabricated gold grids in the environmental chamber of the device (>80% RH, 298 K). Grids were blotted from only the gold side of the grid with glass fiber filter for 5 sec and plunged into liquid ethane. For freezing hemagglutinin with the BIU device, sample (1 µL) was applied to the piezoelectric transducer and liquid was transferred to the grid by energizing the high-frequency generating circuit for 30 msec. An additional 30 msec was allowed for the glass fiber filter to wick sample through the grid before retracting the filter and plunging the grid into the liquid propane/ethane bath. High-speed movies were recorded at 480 frames per second with a rolling shutter using a OnePlus6 mobile phone.

CryoEM data collection

All cryoEM data were acquired at 300 kV with a Thermo Fisher Scientific Titan Krios G3 electron microscope and prototype Falcon 4 camera operating in electron counting mode at 250 frames/sec. The microscope was automated with the *EPU* software package and data collection was monitored with *cryoSPARC Live* (*27*).

3,168 movies were acquired from two grids of apoferritin prepared with BIU. The pixel size was calibrated at 0.816 Å/pixel by fitting a crystal structure of human ferritin L chain (PDB ID: 2FFX) (*28*) into a preliminary 3D map. Movies were collected for 9 sec with 29 exposure fractions, a camera exposure rate of ~3 e^-/pix/sec, and total specimen exposure of ~40 $e^-/Å^2$. A 100 µm objective aperture was used. 1,284 movies were acquired from one grid with hemagglutinin prepared with the CP3. The pixel size was calibrated at 1.03 Å/pixel from a gold diffraction standard. Movies were collected for 9 sec with 29 exposure fractions, a camera exposure rate of ~5 e^-/pix/sec, and a total specimen exposure of ~40 $e^-/Å^2$. No objective aperture was used. 1,556 movies were acquired from one grid with hemagglutinin prepared with the BIU

device. The calibrated pixel size was 1.03 Å. Movies were collected for 9 sec with 29 exposure fractions, a camera exposure rate of ~5 e^-/pix/sec, and a total specimen exposure of ~40 $e^-/Å^2$. No objective aperture was used.

Apoferritin image processing

Exposure fractions were aligned with *MotionCor2* (*29*) within *Relion* (*30*, *31*), using 7×7 patches and a B factor of 500 $pixel^2$ for global alignment and 150 $pixel^2$ for local alignment. Micrographs were then imported into *cryoSPARC* (*27*) and patch CTF estimation was performed. Templates generated from 2D classification during the *cryoSPARC Live* session were used for template selection of particles. 2D classification was used to remove junk particles, resulting in a dataset of 673,794 particle images. An additional round of 2D and 3D classification reduced the dataset to 594,259 particle images. Homogeneous refinement with global and local CTF refinement was then performed and the refined defocus values, Euler angles, and shifts were exported to *Relion*. Particle polishing was done in *Relion* (*32*). The particle images were imported back into *cryoSPARC* for a final round of homogeneous refinement with global and local CTF refinement, producing a 2.0 Å map. Octahedral symmetry was enforced throughout all 3D refinement steps. Transfer of data between *Relion* and *cryoSPARC* were done with *pyem* (10.5281/zenodo.3576630).

Hemagglutinin image processing

Movies were aligned with patch motion correction and patch CTF estimation was performed in *cryoSPARC*. Particle images were selected by blob picking with multiple rounds of 2D classification to remove junk particles. This process resulted in 232,841 hemagglutinin particle images for the specimen prepared with the CP3 grid freezing device. The process gave 378,143 hemagglutinin particle images for the specimen prepared with the BIU device. For 3D structure determination, local motion correction was performed on these particles, followed by repeated rounds of *ab initio* 3D classification with two classes to remove junk particles. The final stack of 128,305 particle images was used to produce a map at 2.9 Å resolution by homogeneous refinement with C3 symmetry enforced and CTF refined globally and locally.

Model building and refinement

A crystal structure of human light chain ferritin (PDB ID: 2FFX) (*28*) was used to start model building for apoferritin and a crystal structure of the influenza A H3N2 hemagglutinin (PDB ID: 3WHE) (*33*) was used to start model building for hemagglutinin. Models were built manually in *Coot* (*34*) and refined with iterative rounds of adjustment in *Coot* and real space refinement with *Phenix* (*35*, *36*). This process was continued until statistics calculated with *Molprobity* (*37*) ceased to improve. Restraints for the ligands were generated with *phenix.ready_set*. The calcium ion in the apoferritin structure was identified by comparison with a previous apoferritin structure (PDB ID: 1Z6O) (*38*). The final map and model were validated using *EMRinger* (*39*) to compare map to model, *cryoSPARC*'s implementation of *blocres* (*40*) to assess map local resolution, the *3DFSC* suite (*16*) to calculate directional resolution anisotropy, and the *SCF* program (*18*) to calculate the sampling compensation factor (SCF), which quantifies how preferred particle orientations contribute to attenuation of the Fourier shell correlation (FSC). Map-to-model FSCs were calculated by converting the model to a map with the *molmap* function in *Chimera* at the Nyquist resolution. A mask was made from this map with *Relion* (after low-pass filtering to 8 Å,

457 extending by 1 pixel, and applying a cosine-edge of 3 pixels), and was applied to the map. Map-
458 to-model FSC was calculated with *proc3d* in *EMAN* (*41*).

Bibliography

1. E. Knapek, J. Dubochet, Beam damage to organic material is considerably reduced in cryo-electron microscopy. *J Mol Biol*. **141**, 147–161 (1980).
2. J. Dubochet, M. Adrian, J. J. Chang, J. C. Homo, J. Lepault, A. W. McDowall, P. Schultz, Cryo-electron microscopy of vitrified specimens. *Q Rev Biophys*. **21**, 129–228 (1988).
3. M. Armstrong, B. Han, S. Gomez, J. Turner, D. A. Fletcher, R. M. Glaeser, Microscale Fluid Behavior during Cryo-EM Sample Blotting. *Biophys. J.* **118**, 708–719 (2020).
4. L. A. Amos, K. Hirose, Studying the Structure of Microtubules by Electron Microscopy. *Methods Mol. Med.* **137**, 65–91 (2007).
5. A. J. Noble, V. P. Dandey, H. Wei, J. Brasch, J. Chase, P. Acharya, Y. Z. Tan, Z. Zhang, L. Y. Kim, G. Scapin, M. Rapp, E. T. Eng, W. J. Rice, A. Cheng, C. J. Negro, L. Shapiro, P. D. Kwong, D. Jeruzalmi, A. des Georges, C. S. Potter, B. Carragher, Routine single particle CryoEM sample and grid characterization by tomography. *Elife*. **7**, e34257 (2018).
6. E. D'Imprima, D. Floris, M. Joppe, R. Sanchez, M. Grininger, W. Kuhlbrandt, Protein denaturation at the air-water interface and how to prevent it. *Elife*. **8**, e42747 (2019).
7. R. M. Glaeser, B. G. Han, R. Csencsits, A. Killilea, A. Pulk, J. H. D. Cate, Factors that Influence the Formation and Stability of Thin, Cryo-EM Specimens. *Biophys. J.* **110**, 749–755 (2016).
8. I. Razinkov, V. P. Dandey, H. Wei, Z. Zhang, D. Melnekoff, W. J. Rice, C. Wigge, C. S. Potter, B. Carragher, A new method for vitrifying samples for cryoEM. *J. Struct. Biol.* **195**, 190–198 (2016).
9. H. Wei, V. P. Dandey, Z. Zhang, A. Raczkowski, W. J. Rice, B. Carragher, C. S. Potter, Optimizing "self-wicking" nanowire grids. *J. Struct. Biol.* **202**, 170–174 (2018).
10. C. R. Marr, S. Benlekbir, J. L. Rubinstein, Fabrication of carbon films with approximately 500 nm holes for cryo-EM with a direct detector device. *J Struct Biol*. **185**, 42–47 (2014).
11. T. Jain, P. Sheehan, J. Crum, B. Carragher, C. S. Potter, Spotiton: A prototype for an integrated inkjet dispense and vitrification system for cryo-TEM. *J. Struct. Biol.* **179**, 68–75 (2012).
12. V. P. Dandey, H. Wei, Z. Zhang, Y. Z. Tan, P. Acharya, E. T. Eng, W. J. Rice, P. A. Kahn, C. S. Potter, B. Carragher, Spotiton: New features and applications. *J. Struct. Biol.* **202**, 161–169 (2018).
13. M. C. Darrow, J. P. Moore, R. J. Walker, K. Doering, R. S. King, Chameleon : Next Generation Sample Preparation for CryoEM based on Spotiton. *Microsc Microanal*. **25**, 994–995 (2019).
14. J. L. Rubinstein, H. Guo, Z. A. Ripstein, A. Haydaroglu, A. Au, C. M. Yip, J. M. Di Trani, S. Benlekbir, T. Kwok, Shake-it-off: A simple ultrasonic cryo-EM specimen preparation device. *Acta Cryst*. **D75**, 632125 (2019).
15. Y. Talmon, The study of nanostructured liquids by cryogenic-temperature electron microscopy - A status report. *J. Mol. Liq.* **210**, 2–8 (2015).
16. Y. Z. Tan, P. R. Baldwin, J. H. Davis, J. R. Williamson, C. S. Potter, B. Carragher, D. Lyumkis, Addressing preferred specimen orientation in through tilting. *Nat. Methods*. **14**, 793–796 (2017).
17. W. F. Tivol, A. Briegel, G. J. Jensen, An improved cryogen for plunge freezing. *Microsc. Microanal.* **14**, 375–379 (2008).
18. P. R. Baldwin, D. Lyumkis, Non-uniformity of projection distributions attenuates

505 resolution in. *Prog. Biophys. Mol. Biol.* **150**, 160–183 (2020).
506 19. J. L. Vilas, H. D. Tagare, J. Vargas, J. M. Carazo, C. O. S. Sorzano, Measuring local-
507 directional resolution and local anisotropy in cryo-EM maps. *Nat. Commun.* **11**, 1–7
508 (2020).
509 20. D. Ashtiani, H. Venugopal, M. Belousoff, B. Spicer, J. Mak, A. Neild, A. de Marco,
510 Delivery of femtolitre droplets using surface acoustic wave based atomisation for cryo-
511 EM grid preparation. *J. Struct. Biol.* **203**, 94–101 (2018).
512 21. X. Feng, Z. Fu, S. Kaledhonkar, Y. Jia, B. Shah, A. Jin, Z. Liu, M. Sun, B. Chen, R. A.
513 Grassucci, Y. Ren, H. Jiang, J. Frank, Q. Lin, A Fast and Effective Microfluidic Spraying-
514 Plunging Method for High-Resolution Single-Particle Cryo-EM. *Structure*. **25**, 663–670
515 (2017).
516 22. S. Kaledhonkar, Z. Fu, H. White, J. Frank, Time-Resolved Cryo-electron Microscopy
517 Using a Microfluidic Chip. *Methods Mol. Biol.* **1764**, 59–71 (2018).
518 23. D. Kontziampasis, D. P. Klebl, M. G. Iadanza, C. A. Scarff, F. Kopf, F. Sobott, D. C. F.
519 Monteiro, M. Trebbin, S. P. Muench, H. D. White, A cryo-EM grid preparation device for
520 time-resolved structural studies. *IUCr J.* **6**, 1024–1031 (2019).
521 24. Z. Lu, D. Barnard, T. R. Shaikh, X. Meng, Gas-assisted annular microsprayer for sample
522 preparation for time-resolved cryo-electron microscopy. *J. Micromechanics*
523 *Microengineering*. **24**, 115001 (2014).
524 25. S. A. Arnold, S. Albiez, N. Opara, M. Chami, C. Schmidli, A. Bieri, C. Padeste, H.
525 Stahlberg, T. Braun, Total Sample Conditioning and Preparation of Nanoliter Volumes for
526 Electron Microscopy. *ACS Nano*. **10**, 4981–4988 (2016).
527 26. S. A. Arnold, S. Albiez, A. Bieri, A. Syntychaki, R. Adaixo, R. A. McLeod, K. N. Goldie,
528 H. Stahlberg, T. Braun, Blotting-free and lossless cryo-electron microscopy grid
529 preparation from nanoliter-sized protein samples and single-cell extracts. *J. Struct. Biol.*
530 **197**, 220–226 (2017).
531 27. A. Punjani, J. L. Rubinstein, D. J. Fleet, M. A. Brubaker, cryoSPARC: Algorithms for
532 rapid unsupervised cryo-EM structure determination. *Nat. Methods*. **14**, 290–296 (2017).
533 28. Z. Wang, C. Li, M. Ellenburg, J. Ruble, J. X. Ho, D. C. Carter, Structure of human ferritin
534 L chain research papers. *Acta Cryst*. **D62**, 800–806 (2006).
535 29. S. Q. Zheng, E. Palovcak, J.-P. Armache, K. A. Verba, Y. Cheng, D. A. Agard,
536 MotionCor2 : anisotropic correction of beam-induced motion for improved cryo-electron
537 microscopy. *Nat. Methods*. **14**, 331–332 (2017).
538 30. S. H. W. Scheres, RELION: implementation of a Bayesian approach to cryo-EM structure
539 determination. *J Struct Biol*. **180**, 519–530 (2012).
540 31. D. Kimanius, B. O. Forsberg, S. H. W. Scheres, E. Lindahl, Accelerated cryo-EM
541 structure determination with parallelisation using GPUs in RELION-2. *Elife*. **5**, e18722
542 (2016).
543 32. J. Zivanov, T. Nakane, S. H. W. Scheres, A Bayesian approach to beam-induced motion
544 correction in cryo-EM single-particle analysis. *IUCrJ*. **6**, 5–17 (2019).
545 33. Y. Iba, Y. Fujii, N. Ohshima, T. Sumida, R. Kubota-koketsu, M. Ikeda, Conserved
546 Neutralizing Epitope at Globular Head of Hemagglutinin in H3N2 Influenza Viruses. *J.*
547 *Virol.* **88**, 7130–7144 (2014).
548 34. P. Emsley, K. Cowtan, Coot: Model-building tools for molecular graphics. *Acta Cryst*.
549 **D60**, 2126–2132 (2004).
550 35. P. D. Adams, P. V. Afonine, G. Bunkóczi, V. B. Chen, I. W. Davis, N. Echols, J. J.

Headd, L. W. Hung, G. J. Kapral, R. W. Grosse-Kunstleve, A. J. McCoy, N. W. Moriarty, R. Oeffner, R. J. Read, D. C. Richardson, J. S. Richardson, T. C. Terwilliger, P. H. Zwart, PHENIX: A comprehensive Python-based system for macromolecular structure solution. *Acta Cryst.* **D66**, 213–221 (2010).

36. P. V. Afonine, B. K. Poon, R. J. Read, O. V. Sobolev, T. C. Terwilliger, A. Urzhumtsev, P. D. Adamsa, Real-space refinement in PHENIX for cryo-EM and crystallography research papers. *Acta Cryst.* **D74**, 531–544 (2018).
37. V. B. Chen, W. B. Arendall, J. J. Headd, D. A. Keedy, R. M. Immormino, G. J. Kapral, L. W. Murray, J. S. Richardson, D. C. Richardson, MolProbity: all-atom structure validation for macromolecular crystallography. *Acta Cryst*. **D66**, 12–21 (2010).
38. A. E. Hamburger, A. P. W. Jr, Z. A. Hamburger, P. Hamburger, P. J. Bjorkman, Crystal Structure of a Secreted Insect Ferritin Reveals a Symmetrical Arrangement of Heavy and Light Chains. *J. Mol. Biol.* **349**, 558–569 (2005).
39. B. A. Barad, N. Echols, R. Y. R. Wang, Y. Cheng, F. Dimaio, P. D. Adams, J. S. Fraser, EMRinger: Side chain-directed model and map validation for 3D cryo-electron microscopy. *Nat. Methods*. **12**, 943–946 (2015).
40. G. Cardone, J. B. Heymann, A. C. Steven, One number does not fit all: Mapping local variations in resolution in cryo-EM reconstructions. *J. Struct. Biol.* **184**, 226–236 (2013).
41. S. J. Ludtke, P. R. Baldwin, W. Chiu, EMAN: semiautomated software for high-resolution single-particle reconstructions. *J Struct Biol*. **128**, 82–97 (1999).

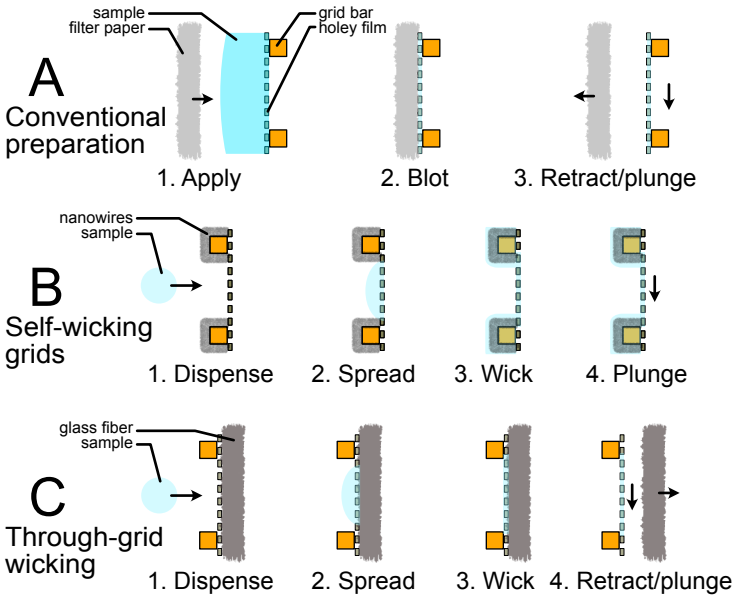

Figure 1

sample

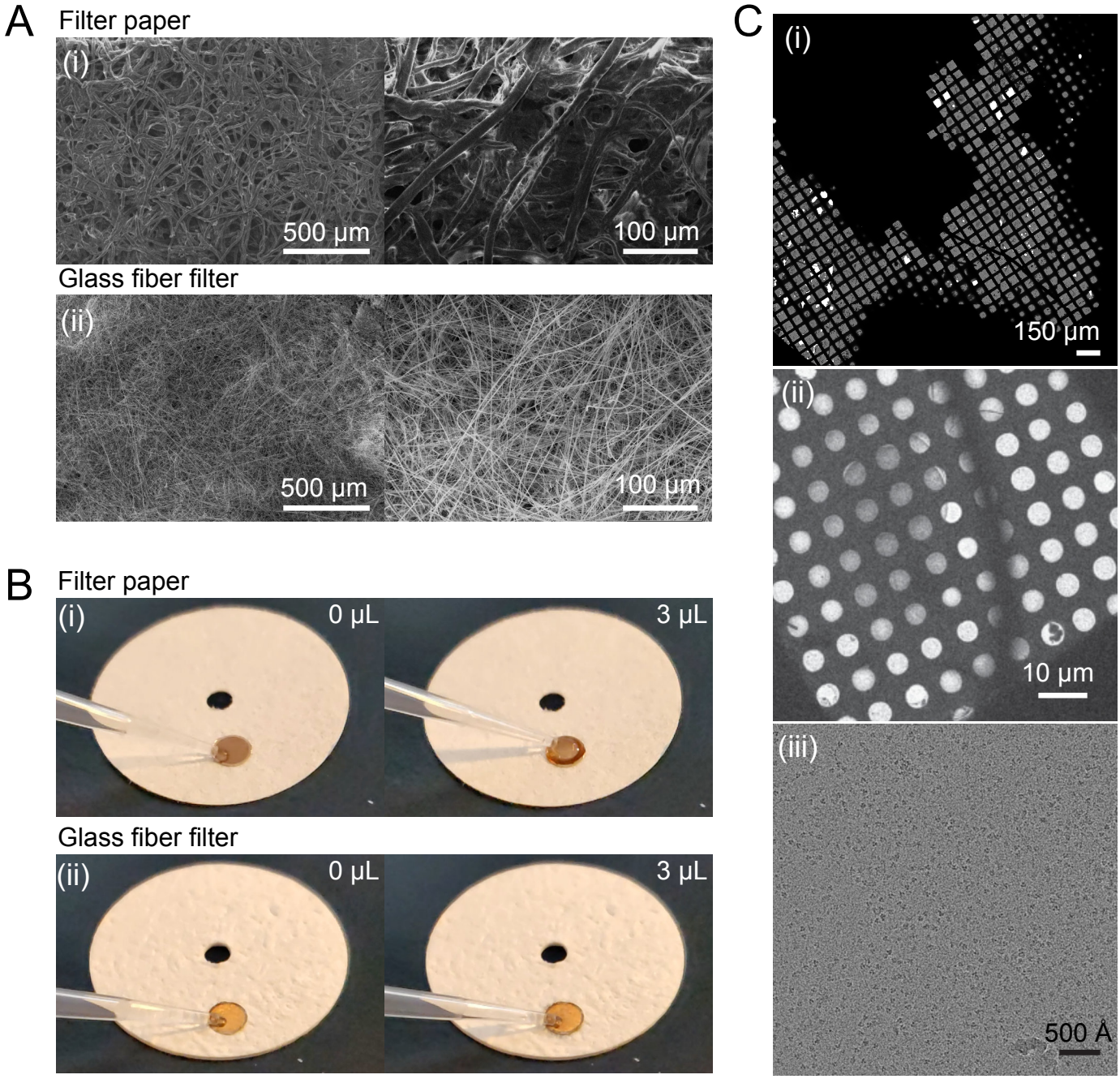
A
Filter paper
(i)
500 µm
100 µm
Glass fiber filter
(ii)
500 µm
100 µm
B
Filter paper
(i)
0 µL
3 µL
Glass fiber filter
(ii)
0 µL
3 µL
C
(i)
150 µm
(ii)
10 µm
(iii)
500 Å

Figure 2

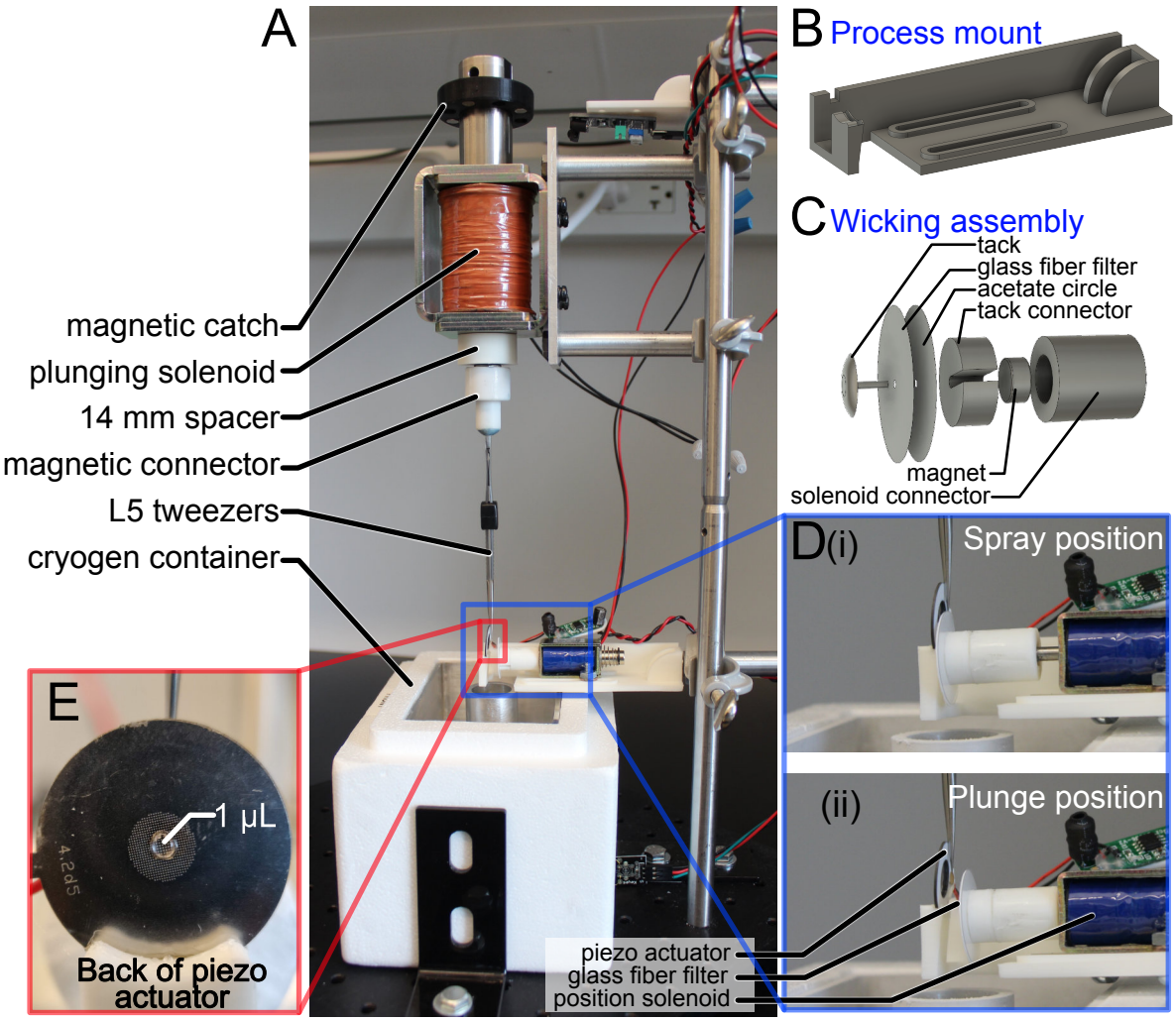
A
magnetic catch
plunging solenoid
14 mm spacer
magnetic connector
L5 tweezers
cryogen container
B Process mount
C Wicking assembly
tack
glass fiber filter
acetate circle
tack connector
magnet
solenoid connector
D(i)
Spray position
(ii)
Plunge position
piezo actuator
glass fiber filter
position solenoid
E
1 μL
Back of piezo actuator

Figure 3

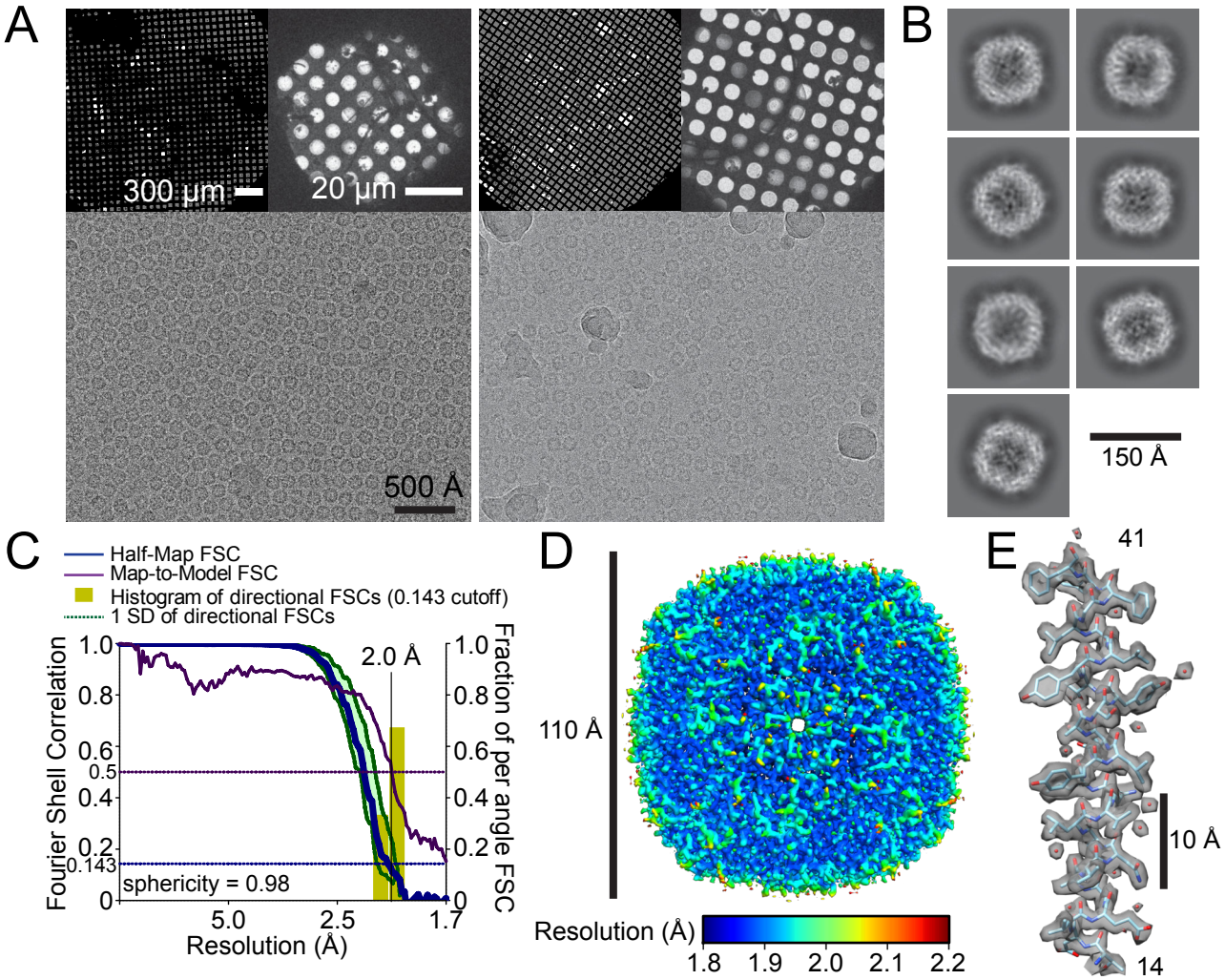
A
300 µm
20 µm
500 Å
B
150 Å
C
Half-Map FSC
Map-to-Model FSC
Histogram of directional FSCs (0.143 cutoff)
1 SD of directional FSCs
Fourier Shell Correlation
Fraction of per angle FSC
2.0 Å
sphericity = 0.98
Resolution (Å)
D
110 Å
Resolution (Å)
1.8
1.9
2.0
2.1
2.2
E
41
10 Å
14

Figure 4

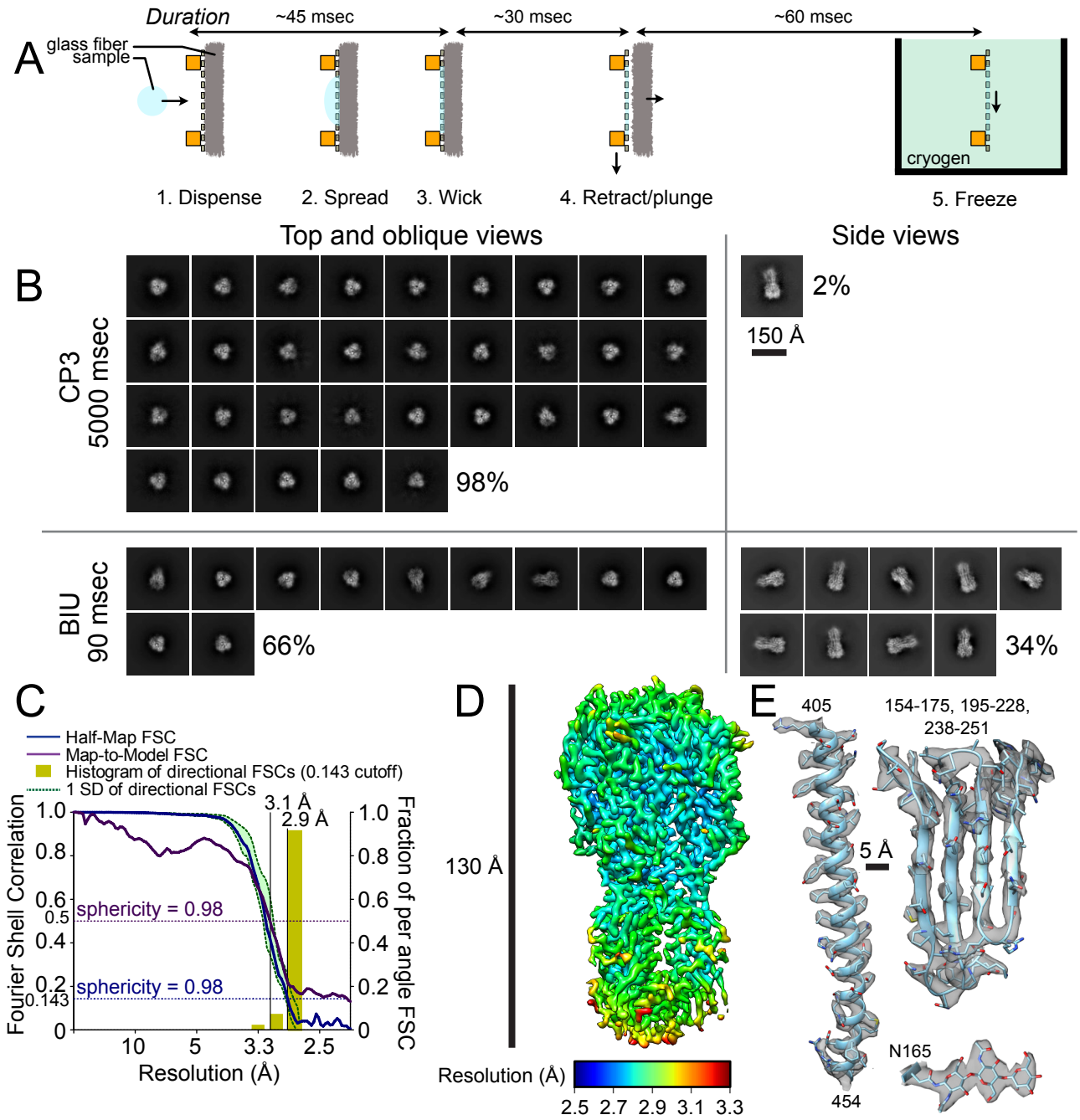
A
Duration
~45 msec
~30 msec
~60 msec
glass fiber
sample
cryogen
1. Dispense
2. Spread
3. Wick
4. Retract/plunge
5. Freeze
B
Top and oblique views
Side views
CP3
5000 msec
98%
2%
150 Å
BIU
90 msec
66%
34%
C
Half-Map FSC
Map-to-Model FSC
Histogram of directional FSCs (0.143 cutoff)
1 SD of directional FSCs
3.1 Å
2.9 Å
sphericity = 0.98
sphericity = 0.98
Fourier Shell Correlation
Fraction of per angle FSC
Resolution (Å)
D
130 Å
Resolution (Å)
2.5 2.7 2.9 3.1 3.3
E
405
154-175, 195-228,
238-251
5 Å
N165
454

Figure 5